Journal of Renewable Materials

Tech Science Press

https://doi.org/10.32604/jrm.2026.02026-0030

ARTICLE

# Nano-Silica Synthesis from Rice Husk Waste and Its Use as a Paper Sheet Anti-Aging Coating with Density Functional Theory (DFT) Insights

**Mona A. El-Sabour, Mohamed El-Sakhawy* and Hebat-Allah S. Tohamy**

Cellulose and Paper Department, National Research Centre, 33 El Bohouth Str., Dokki, Giza, Egypt

*Corresponding Author: Mohamed El-Sakhawy. Email: mm.el-sakhawy@nrc.sci.eg

Received: 25 February 2026; Accepted: 22 July 2026; Published: 23 September 2026

**ABSTRACT:** Paper ages naturally by heat, oxidation, and hydrolysis, which cause a progressive loss of mechanical strength. This study achieved a high yield of 93% amorphous $SiO_2$ from rice husk waste through controlled calcination at 450°C (3 h) and 800°C (2 h), alkaline extraction with 2.5 N NaOH, acid precipitation with 1 N HCl and freeze-drying. The resulting nano-silica particles were incorporated into a 3% w/v hydroxyethyl cellulose (HEC) binder to prepare a 2% w/v impregnation solution, which was applied to paper sheets by soaking for 0–20 min. Structural analyses (FTIR, XRD, SEM) confirmed the successful preparation of hydroxylated amorphous silica and uniform deposition on paper fibers. Optimal mechanical performance was achieved at soaking times of 10–15 min, where a maximum weight percent gain (WPG) of 35.27% was recorded. Post-aging tensile strength and elongation improved by up to 25% and 94%, respectively, compared to uncoated paper. The limiting oxygen index (LOI) values increased from 18.0 to 22.3 vol.%, indicating improved flame retardancy. Density Functional Theory (DFT) calculations revealed that the nano-silica coated paper exhibited a wider HOMO–LUMO energy gap (1.342 to 1.803 eV) and higher chemical hardness (0.671 to 0.902 eV), confirming enhanced chemical stability and reduced susceptibility to oxidative degradation. This study combine bio-derived nano-silica from rice husk waste with DFT quantum chemical analysis to elucidate the molecular-level anti-aging mechanism of a paper coating system. The study demonstrates a sustainable route for converting agricultural waste into functional nanomaterials for paper preservation and performance enhancement.

**KEYWORDS:** Flame retardancy; paper aging; nano-silica; rice husk valorization; DFT calculations; sustainable coatings

## 1 Introduction

Paper remains one of the most essential materials in modern society, being used extensively for documentation, packaging, education, and communication. Due to its indispensable use in printing, labeling, and biodegradable packaging, the demand for paper is still growing worldwide despite the rapid shift toward digital technology. Maintaining the mechanical performance of paper products and extending their service life in a variety of environmental conditions has become more important due to the rising use of paper goods, particularly in packaging and sanitary applications [1].

However, over time, the appearance of paper changes and its mechanical properties significantly deteriorate due to environmental and thermal aging. The main components of paper, cellulose fibers, undergo hydrolytic, oxidative, and thermal deterioration more quickly when exposed to light, humidity, and air pollution [2].

Paper becomes more likely to tear and crumble as a result of this deterioration, which also leads to discoloration, brittleness, and a weakened structure. Acidic paper, commonly found in older materials,

deteriorates faster due to the accelerated breakdown of cellulose. These processes are accelerated by high humidity and temperature, which reduce elasticity, tensile strength, and folding endurance. The lifespan and utility of paper documents and artifacts are greatly impacted by these changes over time, making appropriate handling and storage methods necessary to mitigate the impacts of aging [3].

Several stabilization methods have been investigated, including surface coatings, filler inclusion, and deacidification, to minimize these effects of aging [4].

Recent advances in materials science have introduced a range of novel stabilizing strategies aimed at improving the mechanical and barrier properties of paper and biodegradable films, addressing their inherent limitations such as high-water sensitivity, low tensile strength, and susceptibility to thermal and oxidative degradation [5]. Surface coating strategies using biopolymers such as chitosan, zein, and polyhydroxyalkanoates (PHA) form dense, continuous layers that dramatically reduce oxygen permeability and moisture vapor transmission without compromising end-of-life biodegradability [6]. Cross-linking treatments employing green agents like tannic acid, citric acid, or enzymatic systems such as laccase and transglutaminase introduce covalent bonds within polymer networks, improving water resistance and structural integrity by over 1.5-fold in some formulations [7]. Layer-by-layer (LbL) assembly represents an emerging and highly tunable technique in which alternating polyelectrolyte layers are deposited onto film surfaces to engineer multifunctional coatings with controlled barrier properties against grease, oxygen, and humidity [8]. Deacidification treatments and hybrid polymer-filler systems, including blends of PLA, PBAT, and starch with reactive compatibilizers, further fine-tune flexibility, interfacial adhesion, and degradation resistance for sustainable packaging applications [9]. Emerging techniques such as atmospheric cold plasma (ACP) surface treatment introduce reactive nitrogen- and oxygen-containing functional groups onto film surfaces, enhancing tensile strength and creating more tortuous vapor diffusion pathways through entirely solvent-free, environmentally friendly processing [10]. Hydrophobization strategies incorporating bio-waxes, esterified lignin, or lipid-based additives further improve water contact angles and grease resistance, expanding the functional range of cellulosic substrates for food packaging [11].

Protective coatings that act as strong barriers against moisture, oxygen, and light have been made possible by recent developments in nanotechnology. These nano-coatings successfully slow down degradation processes because of their large surface area and unique physicochemical characteristics [12]. Nanoparticles such as cellulose nanocrystals (CNC), nano-clays like montmorillonite, and graphene oxide are embedded into biopolymer matrices to create tortuous diffusion pathways that impede moisture and gas permeation while enhancing stiffness and tensile performance, with CNC-based films achieving tensile strengths as high as 185 MPa [13].

Specifically, because of their thermal stability, high compatibility with cellulose fibers, low toxicity, and abundant surface silanol groups capable of hydrogen bonding, nano-silica particles ($SiO_2$) have been identified as useful protective and reinforcing agents [14]. In the context of green chemistry and the circular economy, the sustainable synthesis of nano-silica particles from agricultural waste sources has grown in importance. The global production scale of rice husk exceeds 150 million tons per year, with its silica ($SiO_2$) composition ranging between 15–20 wt.%, making it an abundantly available and chemically valuable agricultural byproduct for the synthesis of high-purity silica-based nanomaterials [15]. The use of agricultural waste as a silica source not only offers a sustainable alternative to synthetic chemicals but also contributes to environmental protection and circular material utilization [16]. The outcomes are expected to advance the development of eco-friendly, high-performance coatings for paper-based materials with extended lifetime and resistance to degradation under aging and thermal conditions. High-purity amorphous silica with a large surface area and a high density of silanol groups can be produced from rice husk ash by controlled burning, alkaline extraction, and acid precipitation [17]. According to recent research, nano-silica can be added to

polymeric matrix or coatings to improve the mechanical and barrier qualities of paper and biodegradable films. For instance, cellulose-based sheets' strength and hydrophobicity were successfully increased using bio-derived silica from rice husk, while coatings treated with silica showed enhanced resistance to oxidation and moisture absorption [18]. These results demonstrate the potential of silica produced from rice husks as a useful ingredient for enhancing the stability and durability of paper. However, the majority of earlier research has concentrated on the issues of physical reinforcement, while fewer studies examined the quantum-chemical basis of stability or connected silica coating to both mechanical and flame-retardant enhancement in a unified framework. In this regard, molecular-level insights into the stability, reactivity, and electrical characteristics of materials can be obtained by Density Functional Theory (DFT) simulations. In order to correlate microscopic electronic stability with macroscopic anti-aging performance, DFT can predict the chemical hardness, softness, and energy gap of coated vs. uncoated paper systems by examining the energies of the highest occupied (HOMO) and lowest unoccupied (LUMO) molecular orbitals [19].

The goal and novelty of this study lie in integrating green synthesis of rice-husk-derived nano-silica, a simple impregnation coating strategy, experimental validation of anti-aging and flame-retardant performance, and DFT-based molecular interpretation within a single framework.

This work offers a novel combination of experimental and theoretical approaches to demonstrate a sustainable synthesis of bio-derived nano-silica from rice husk waste. This silica can specifically be utilized for paper anti-aging and flame retardancy rather than just to enhance both the mechanical and chemical stability of paper materials.

Further research should investigate long-term natural aging, coating uniformity, pilot-scale coating trials, surface chemistry mapping by XPS, precise silica quantification by TGA and elemental analysis, and the exploration of barrier properties, including water vapor transmission rate and oil resistance, for potential packaging applications.

## 2 Experiment

### *2.1 Materials*

All chemicals such as hydroxy ethyl cellulose (HEC), sodium lauryl sulphate (SLS), hydrochloric acid, and sodium hydroxide were analytical grade and purchased from Sigma-Aldrich and used without further purification. Rice husk (RH) was collected from a local rice mill in Egypt. It was first washed with tap water to remove dirt and water-soluble substances, and then dried in a sunny place for 72 h.

### *2.2 Paper Substrate*

The paper sheet was kindly supplied by Rakta Company, Egypt (basic weight 80 g/m$^2$, consisting of bleached rice straw pulp (60%) blended with bleached bagasse pulp (20%) and bleached softwood pulp (20%).

### *2.3 Extraction of Silica from RH*

The extraction of silica from RH conditions was chosen based on optimized yields reported in previous literature to ensure maximum silica extraction [20]. In a muffle furnace, the dry rice husk was calcined at 450°C for 3 h, then at 800°C for 2 h to ensure removal of organics and production of amorphous silica-rich ash. The resulting white ash was refluxed with 2.5 N NaOH (this concentration has been shown to be effective for silica dissolution from rice husk ash) in a liquor ratio of 1:10 for three hours while being stirred to allow sufficient silica conversion to sodium silicate. The resulting solution was filtered and washed with water to remove impurities. The sodium silicate solution was allowed to cool to ambient temperature, followed

by titration with 1 N HCl under vigorous stirring. The solution was neutralized and then left to gradually precipitate silica gel. To avoid the creation of large aggregates, a slow titration was carried out while vigorously stirring. The silica gel was filtered, washed, and freeze-dried to remove water. The freeze-dried silica appeared as a fine white nano-silica powder with a yield of 93% from the ash [20]. Noting that while 93% yield is high, variations in NaOH molarity and burning temperature (500°C–700°C) can affect the yield, amorphous nature and surface area of the silica [21].

### *2.4 Preparation of Impregnation Solutions*

An impregnation solution was prepared by dissolving HEC (3% w/v) in distilled water with continuous stirring until it became homogeneous. NaOH (0.5% w/v) was added to the solution, followed by nano-silica and an anionic surfactant (SLS, 15% by weight relative to silicate). The mixture was stirred and sonicated for 30 min to ensure homogeneous dispersion.

### *2.5 Coating of Paper Sheets with the Impregnation Solution*

Paper sheets were pre-dried at 90°C for 6 h to activate the surface and remove moisture. The coating of paper samples was performed by soaking them in a 2% (w/v) impregnation solution. Soaking time varied from 0 to 20 min (selected after preliminary trials to capture coating uptake behavior without over-saturation, coating leaching or decrease in mechanical integrity). Soaking time directly correlates with the diffusion of the HEC/silica matrix into the fiber network; longer times (up to 15 min) increase the $SiO_2$ loading until saturation is reached. Soaking allows the impregnation solution to be deposited on the paper sheet surface in the form of thin layers and facilitates the diffusion of colloidal silicate into paper. Following soaking, the paper sheets were pressed between two tissue papers to remove excess solution and then dried at 40°C to constant weight. This promotes the creation of a silicate framework in the paper by allowing water to evaporate. Prior to and following coating, the original dried weight was recorded. All paper samples were conditioned for 24 h at 23°C and 50% humidity prior to characterization tests.

### *2.6 Weight Percent Gain (WPG)*

The WPG of the samples was determined on an oven-dried weight basis as shown in Eq. (1).

$$WPG = ((W1 - W0)/W0) \times 100\% \quad (1)$$

where W0 and W1 are oven-dry weights before and after coating, respectively.

### *2.7 Accelerated Aging*

The paper sheets were submitted to accelerated aging in an oven at 140°C for 2 h.

### *2.8 Characterization of Paper Sheets*

Tensile strength was measured according to TAPPI (T494-06) standard method using a universal testing Machine model 4201.

The limiting oxygen index (LOI) of the paper sheets was determined using a flammability testing CSI oxygen index meter (Atlas) in accordance with ASTM D-2863. The paper sheets had dimensions of 100 mm × 52 mm × 0.3 mm, and the flame height ranged from 6 to 25 mm [22].

SEM images were obtained using a Quanta/250-FEG microscope running at an accelerating voltage of 30 kilovolts. Using a Bruker diffractometer, samples of the X-ray diffractions were examined at 40 kV, 40 mA CuK radiation source with a second monochromator ($\lambda$ = 1.5405 Å).

FTIR spectra were obtained using a Mattson 5000 spectrometer with potassium bromide pellets.

### *2.9 DFT Calculations*

Density functional theory (DFT) calculations were performed using the Gaussian 09W software package. Geometry optimizations were carried out at the B3LYP/6-31G(d) level of theory utilizing the Berny algorithm. To simulate the interaction between the paper substrate and the nano-silica coating, a molecular model was constructed using a cellobiose unit (comprised of two $\beta$-D-glucopyranose units) to represent the cellulose surface. The silica component was explicitly modeled as a hydrated dimeric silicate cluster with the structure $HO–Si(OH)_2–O–Si(OH)_2OH$. This specific configuration was chosen to reflect the amorphous nature of the extracted nano-silica, incorporating both the siloxane (Si–O–Si) internal linkage and multiple terminal silanol (Si–OH) groups responsible for hydrogen bonding with the cellulose chain. By utilizing a dimeric cluster rather than a monomeric unit, the model accounts for the electronic effects of the silica backbone, providing a more realistic calculation of the HOMO-LUMO energy gap and the resulting chemical hardness of the coated paper system.

A series of electronic parameters was investigated to characterize the ground-state properties and interaction energies. These parameters included total energy (ET), the energy of the highest occupied molecular orbitals $E_{HOMO}$, the energy of the lowest unoccupied molecular orbitals $E_{LUMO}$, the energy gap ($E_g$), the absolute hardness ($\eta$), the dipole moment ($\mu$), the absolute softness ($\sigma$), and the chemical softness (S) via Eqs. (2)–(5) [23]. All energy values were extracted in Hartrees and converted to electron volts (1 Hartree = 27.2114 eV) for physical interpretation.

$$E_g = (E_{LUMO} - E_{HOMO}) \tag{2}$$

$$\eta = \frac{(E_{LUMO} - E_{HOMO})}{2} \tag{3}$$

$$\sigma = \frac{1}{\eta} \tag{4}$$

$$\mathrm{S} = \frac{1}{2\eta} \tag{5}$$

## 3 Results and Discussions

### *3.1 FTIR Spectroscopy of Nano-Silica*

The FTIR spectrum of synthesized nano-silica derived from rice husk ash (Fig. 1) displays all diagnostic absorption bands corresponding to Si–O–Si and Si–OH vibrations of amorphous $SiO_2$. The dominant feature of the spectrum is the intense, broad absorption band centered at 1090 $cm^{-1}$, which is attributed to the asymmetric stretching vibration of Si–O–Si linkages within the siloxane network. This band is widely recognized as the principal fingerprint of amorphous silica and has been consistently reported in the range of 1050–1100 $cm^{-1}$ for bio-derived silica obtained from agricultural residues [24]. The observed broadening of this band, compared to the sharp and narrow absorption seen in crystalline quartz, is a direct consequence of the short-range structural disorder and variable Si–O–Si bond angle distribution that define the amorphous state, in full agreement with previous characterizations of rice husk ash-derived silica reported by Fernandes et al. [25]. The symmetric stretching mode of Si–O–Si appears at 800 $cm^{-1}$, while the Si–O bending deformation is well-defined at 470 $cm^{-1}$, which has been consistently documented across multiple studies on amorphous silica nanoparticles derived from rice husk [25]. The intensity and breadth of the silanol band reflect a high surface density of reactive hydroxyl groups, a feature that is characteristic of gel-derived or wet-chemistry-produced nano-silica. The presence of abundant surface silanol groups

distinguishes bio-derived nano-silica from thermally crystallized silica polymorphs and is responsible for its strong affinity toward cellulose fibers through hydrogen bonding interactions [26]. Collectively, the co-occurrence and spectral positions of these four silica-specific bands; at 1090, 800, and 470 $cm^{-1}$; are fully consistent with the FTIR signatures reported in the literature for amorphous, hydroxylated nano-silica of both synthetic and bio-derived origin, confirming the formation of the target material through the present synthesis route.

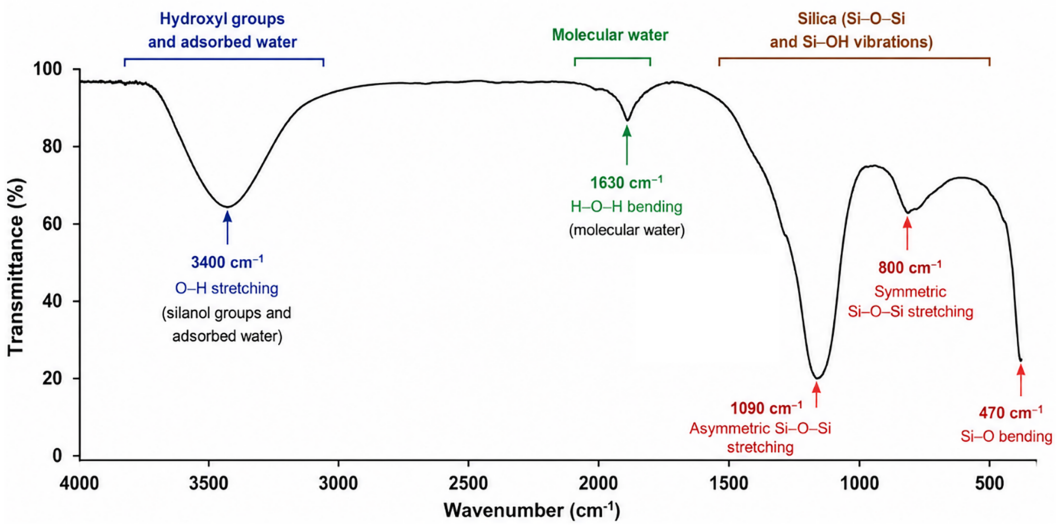


**Figure 1:** FTIR spectrum of amorphous nano-silica synthesized from rice husk ash via alkaline extraction (2.5 N NaOH) and acid precipitation (1 N HCl), followed by freeze-drying.

A broad band at 3400 $cm^{-1}$ is attributed to the O–H stretching vibrations from adsorbed water or surface silanol hydroxyl groups, whereas the band near 1630 $cm^{-1}$ corresponded to the H–O–H bending of molecular water [27], further corroborating the hydrophilic and highly hydroxylated character of the nanoparticle surface, a well-established feature of high-surface-area amorphous silica. The simultaneous observation of both the 3400 and 1630 $cm^{-1}$ bands is diagnostic of nano-silica produced through wet chemical routes, rather than through high-temperature calcination processes, which typically collapse silanol groups into siloxane bridges and reduce surface hydroxyl density [28]. This behavior aligns closely with findings reported that alkaline-extracted, acid-precipitated silica from rice husk retains a markedly higher silanol group density compared to thermally calcined silica [25].

Notably, no absorption bands assignable to organic residues from the rice husk matrix (e.g., C–H stretching at 2850–2950 $cm^{-1}$, C=O stretching at ~1730 $cm^{-1}$, or aromatic C=C stretching at ~1510 $cm^{-1}$ attributable to lignin) are detected, confirming the effective removal of organic matter during the alkaline extraction and calcination steps. The absence of these lignocellulosic bands is an important indicator of product purity that has been used as a quality criterion in previous studies on bio-derived nano-silica [29]. The spectral profile observed here is in excellent agreement with those reported for silica extracted from rice husk ash under comparable alkaline and acid precipitation conditions, which identified the same set of characteristic absorption bands and likewise noted the complete absence of carbonaceous impurity signals as evidence of successful purification [25].

### *3.2 XRD Analysis*

The XRD pattern of the synthesized nano-silica (Fig. 2) shows a single broad diffraction peak centered at approximately 22° (2$\theta$), with no superimposed sharp reflections anywhere in the recorded 2$\theta$ range. This broad amorphous peak is the defining diffractometric feature of disordered $SiO_2$ and arises from the short-range coherence of Si-O-Si tetrahedral units in the absence of long-range three-dimensional periodicity [30]. The position of the amorphous maximum near 22°, consistent with the Si–O–Si mean bond length distribution in amorphous silica networks as established by X-ray and neutron scattering studies [31]. Critically, the diffractogram shows a complete absence of any sharp reflections that could be attributed to crystalline silica polymorphs: no quartz peaks (the strongest reflection at 2$\theta$ = 26.65°, JCPDS card no. 46-1045), no cristobalite reflections (strongest at 2$\theta$ = 21.8° and 36.0°), and no tridymite signatures are observed [32].

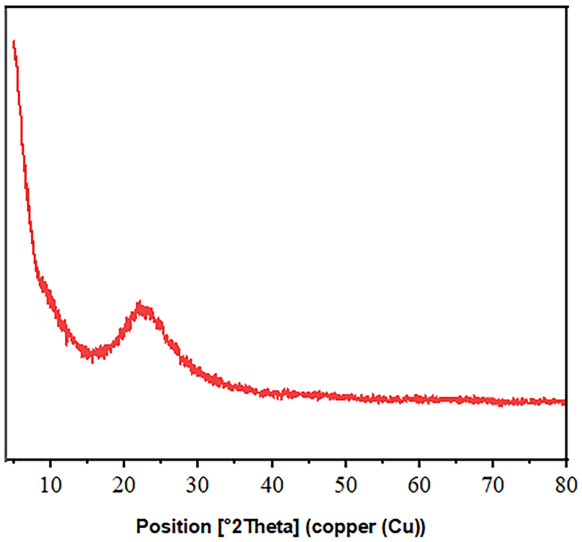


**Figure 2:** XRD of nano-silica synthesized from rice husk ash by controlled calcination (450°C/3 h then 800°C/2 h), alkaline extraction, and acid precipitation.

This is particularly significant because rice husk ash processed at elevated temperatures can undergo partial crystallization to yield $\alpha$-quartz or $\beta$-cristobalite if calcination is conducted at or above 900°C for prolonged durations [33]. The absence of such crystalline phases in the present product confirms that the synthesis conditions were effective in preserving the amorphous network structure throughout processing. This outcome is consistent with earlier reports by Kalapathy et al., who demonstrated that alkaline extraction of silica from rice husk ash below 700°C followed by acid gelation consistently produces XRD-amorphous precipitates, in contrast to the mixed amorphous-crystalline products obtained by direct dry-processing at higher temperatures [34]. Furthermore, the peak position and profile shape of the observed amorphous halo are in close agreement with reference XRD patterns reported for colloidal and precipitated amorphous silica nanoparticles, including commercial fumed silica (Aerosil® ) and Stöber-process silica spheres, both of which display the characteristic broad reflection centered near 22° [35]. The amorphous structure confirmed here is highly desirable for coating and surface modification applications because amorphous $SiO_2$ possesses isotropic surface chemistry, and higher chemical reactivity than crystalline polymorphs. Taken together with the FTIR data, the XRD analysis definitely confirms that the material produced in this study is phase-pure amorphous nano-silica, free of crystalline impurities, and structurally consistent with high-quality bio-derived silica nanoparticles reported in the literature.

### *3.3 DFT Calculations and Theoretical Insights*

Density Functional Theory (DFT)-based calculations were used to examine the electronic stability of uncoated and nano-silica-coated paper sheets. The difference between LUMO and HOMO energies ($E_{LUMO} - E_{HOMO}$) represents the energy gap ($E_g$), a crucial measure of chemical stability. Greater energy gaps indicate reduced reactivity and increased resistance to degradation [36].

The most compelling evidence of reinforcement lies in $E_g$, which effectively measures the paper's chemical barrier. The observed increase from 1.3420 eV in the blank paper to 1.8032 eV in the coated system, according to the DFT results (Table 1, Fig. 3), suggests better electronic and chemical stability [37].

**Table 1:** Quantum chemical parameters derived from DFT calculations for the uncoated- and the nano-silica-coated paper model.

| DFT | Blank Paper | Paper Coated with Silicate |
|---|---|---|
| ELUMO (eV) | −3.4123 | −4.5862 |
| EHOMO (eV) | −4.7543 | −6.3895 |
| $E_g$ (eV) | 1.3420 | 1.8032 |
| ET (au) | −1208.88 | −2298.21 |
| $\mu$ (Debye) | 12.63 | 19.55 |
| $\eta$ (eV) | 0.6710 | 0.9016 |
| $\sigma$ (eV) | 1.4903 | 1.1091 |
| S (eV) | 0.7452 | 0.5546 |

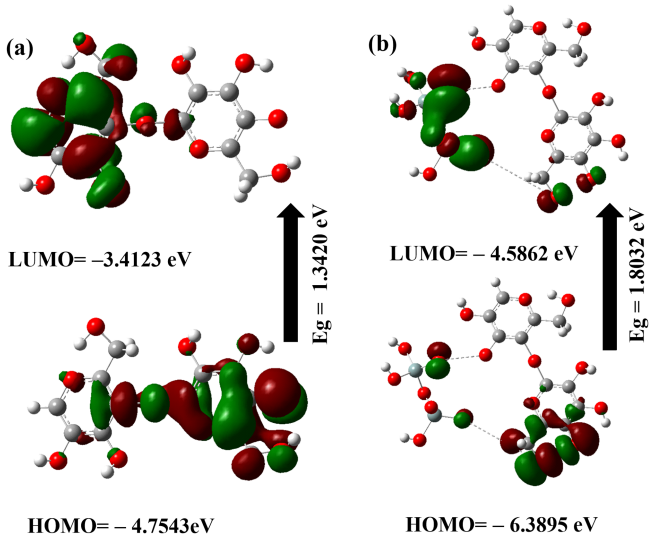


**Figure 3:** DFT-optimized molecular geometries and HOMO-LUMO frontiers orbital distributions for (**a**) the cellobiose model representing the cellulose substrate surface and (**b**) the cellobiose-dimeric silica cluster assembly, modeling the nano-silica-coated paper.

In quantum terms, a larger energy gap means the electrons are more tightly held and less likely to participate in unwanted chemical reactions. This is further validated by the rise in $\eta$ from 0.6710 to 0.9016 eV. This shift indicates that the coating enhances the electronic hardness of the material, making it more resistant to oxidative attacks and radical formation, which typically drive the aging process [38]. Complementing

this increase in hardness is a significant decrease in the S value, which dropped from 0.7452 to 0.5546 eV. While a soft molecule is highly reactive and easily distorted by external stressors like heat or humidity, a harder system is less reactive and more structurally stable. By lowering the softness, the nano-silica coating essentially toughens the molecular framework, providing a theoretical explanation for the paper's enhanced resistance to the thermal degradation observed during the 140°C accelerated aging tests.

The electronic integration of the coating is best illustrated by the dipole moment ($\mu$), which rose from 12.63 Debye for blank paper to 19.55 Debye for the coated system. This rise represents an intensified charge polarization at the interface where the silica's silanol (Si–OH) groups meet the cellulose fibers. This stronger electronic pull confirms that the nano-silica is not merely a superficial layer but is electronically coupled with the paper, creating a unified, reinforced matrix [39]. This synergy is anchored by the ET, which shifted to a much more negative value (–2298.21 au).

Overall, the DFT data confirms the experimental finding that nano-silica coating enhances the paper's chemical stability and anti-aging performance against external factors like heat or light by strengthening the fiber network and reducing electronic reactivity.

### *3.4 Morphological Observations*

Clear morphological variations between blank and nano-silica-coated papers were observed in the SEM micrographs (Fig. 4). A typical fibrous, porous network of cellulose with visible gaps and randomly aligned fibers is observed in the uncoated paper (Fig. 4a). The surface appears relatively rough due to the natural texture and intersections of untreated cellulose fibers. High permeability and the capacity for fluids or particles to penetrate the sheet are shown by the numerous visible pores and voids.

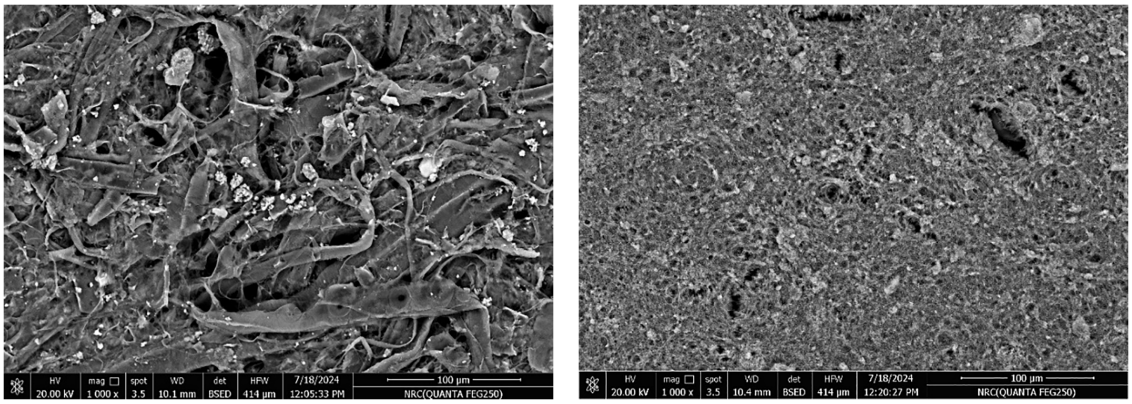


**(a)** **(b)**

**Figure 4:** SEM micrographs of (**a**) uncoated blank paper and (**b**) paper coated with nano-silica/HEC impregnation solution (2% w/v, soaking time 15 min).

On the other hand, the coated paper (Fig. 4b) exhibits uniformly distributed nano-silica particles over and between fibers, resulting in smoother fiber surfaces. By filling in the gaps and spaces between the fibers, these nanoparticles formed a continuous, compact coating layer that improved surface integrity. The silica coating increased the paper's overall mechanical strength, decreased porosity, and strengthened inter-fiber bonding [40]. Such morphological modifications are consistent with the improved tensile and aging performance discussed below.

### *3.5 Mechanical Properties and Weight Percent Gain (WPG)*

In paper industry, the mechanical structure of the final treated paper is greatly influenced by the kind and composition of the treating mixture as well as the blank paper. The properties that characterize how paper resists applied loads or forces are referred to as mechanical properties. To guarantee optimal performance and functionality, several treatment combinations can be mixed for various purposes, such as high-quality printing, magazine production, packaging, or hygiene paper [41].

The results presented in Table 2 indicate that the Weight Percent Gain (WPG) increased with increasing soaking time from 2 to 15 min. The WPG increased up to 35.27%, then decreased beyond 15 min likely due to over-saturation and partial leaching of the coating and cellulose components into the soaking medium. This increase is attributed to the presence of silicate particles within the paper matrix. WPG was used as an indirect $SiO_2$ loading indicator, future work will include TGA, XPS, and elemental mapping for precise quantification of silica loading and coating chemistry.

**Table 2:** Effect of soaking time in a 2% w/v nano-silica/HEC impregnation solution on the mechanical properties of paper sheets before and after accelerated aging.

| Soaking Time, min. | Wt. Gained, % | Tensile Strength, b Mpa | Tensile Strength, a Mpa | Elongation, b % | Elongation, a % | Young's Modulus, b MPa | Young's Modulus, a MPa |
|---|---|---|---|---|---|---|---|
| 0 | 0 | 12.87 | 11.41 | 2.88 | 2.58 | 1702.49 | 1498.55 |
| 2 | 22.65 | 13.79 | 12.74 | 3.47 | 3.19 | 1257.98 | 1202.41 |
| 5 | 26.16 | 13.75 | 13.19 | 4.78 | 4.43 | 904.85 | 865.38 |
| 10 | 27.45 | 14.80 | 14.28 | 4.08 | 3.98 | 744.34 | 712.82 |
| 15 | 35.27 | 12.56 | 12.18 | 5.14 | 5.01 | 610.00 | 584.51 |
| 20 | 26.29 | 11.50 | 11.20 | 3.92 | 3.81 | 580.00 | 556.80 |

Note: b: Before aging & a: After aging at 140°C for 2 h.

The degree of inter-fiber bonding and the distribution of the fibers within the sheet determine the strength of the paper. The strength of this bonding, which begins with the creation of hydrogen bonds between fibers, depends on both the intrinsic strength per unit area and the fiber contact area [42].

Tensile strength of paper is a measure of how much stretching or pulling force it can withstand before breaking. It's a key property for determining paper's suitability for various applications like packaging and is measured by applying force until the paper ruptures [43].

Mechanical testing results (Table 2, Fig. 5) reveal that tensile strength and elongation increase with soaking time up to 10–15 min, achieving maximum improvements of 15% and 78.47% for tensile strength and elongation before aging; while it was 25% and 94% for tensile strength and elongation after aging, respectively, compared to the blank paper. The Young's modulus decreases slightly, indicating improved flexibility and reduced brittleness [44].

The creation of hydrogen bonds between the hydroxyl groups of cellulose fibers and the surface silanol (Si–OH) groups of adsorbed nano-silica is responsible for this improvement. Hydroxyethyl cellulose (HEC) also contributes by creating thin coatings that connect the fibers and encourage cohesive bonding. Consequently, the treated sheets show better load distribution and greater inter-fiber adhesion [45].

Long soaking times (>15 min) caused mechanical characteristics to slightly deteriorate because of excessive particle deposition, which disrupted fiber-fiber contact and reduced flexibility. This finding is consistent with research showing that too much filler can weaken mechanical integrity and prevent fiber bonding [46].

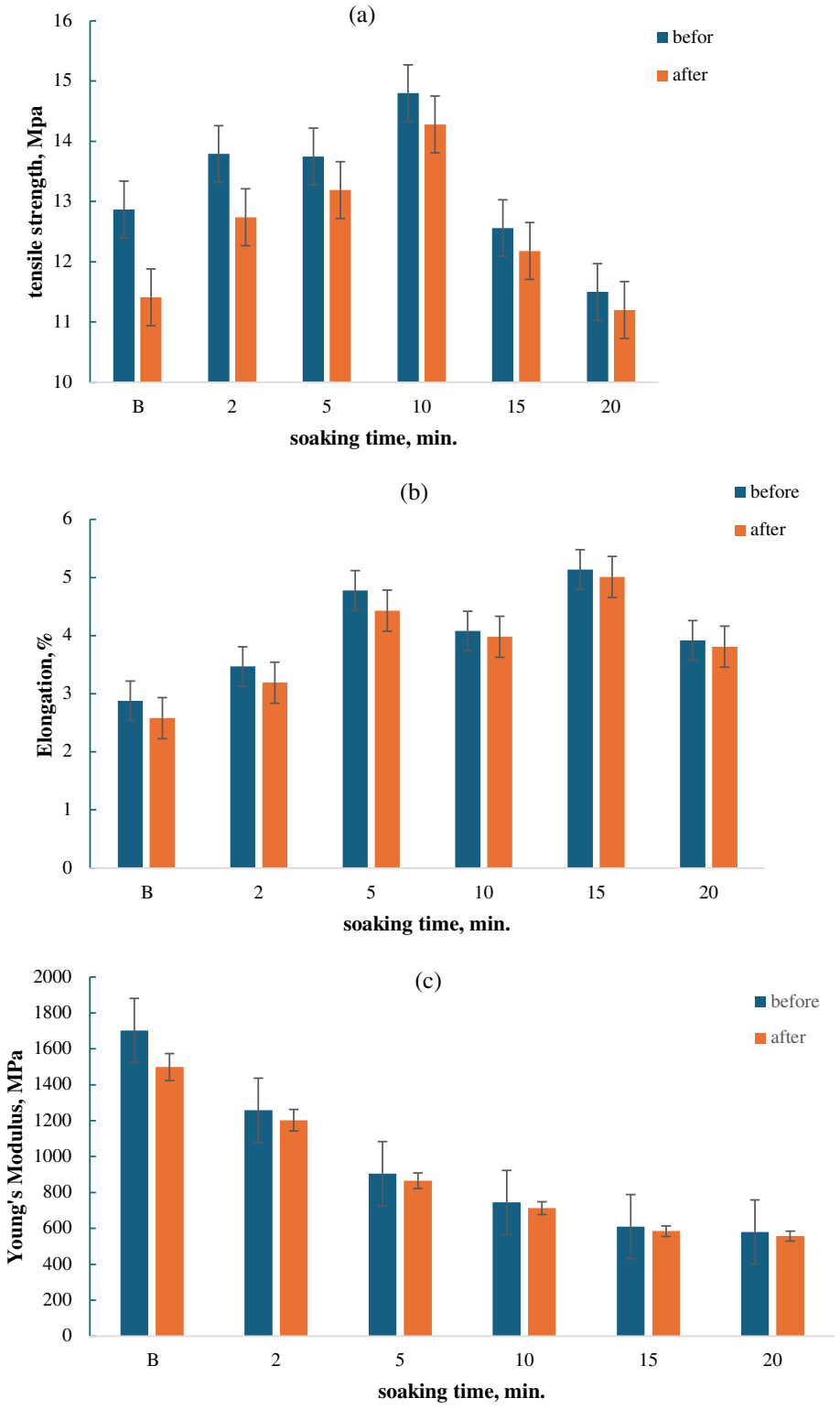


**Figure 5:** Mechanical properties of paper sheets impregnated with nano-silica/HEC solution (2% w/v, soaking times 0–20 min), measured before and after accelerated aging (**a**): tensile strength, (**b**): elongation, (**c**): young's modulus.

### *3.6 Aging Study and Anti-Aging Performance*

Paper sheets are subjected to several fundamental deterioration processes. Under normal storage conditions, these processes are very slow, yet eventually they result in well-known aging effects such as yellowing and weakness.

Hydrolytic, oxidative, and thermal degradation processes are the main causes of paper aging. These events result in the scission of cellulose chains and the formation of carbonyl and carboxyl groups, which weaken the paper [47]. The durability of the coated and uncoated sheets was assessed by artificial aging at 140°C for two hours.

All samples showed decreased mechanical strength after aging; however, the paper coated with nano-silica maintained far greater tensile strength and elongation than the blank. Tensile strength, elongation, and Young's modulus decreased by 11.34%, 10.42%, and 11.9% for the blank paper, whereas decreases of only 3.51%, 2.45%, and 4.23% were observed for the coated paper after 10 min of soaking. The percentage retention of tensile strength after accelerated aging (140°C, 2 h) for coated and uncoated papers are about 96.7 and 88.6, respectively.

These findings demonstrated that nano-silica coating effectively mitigates aging-induced deterioration by forming a barrier that reduced the passage of moisture and oxygen, delayed thermal deterioration, and stabilized the cellulose network.

### *3.7 Flammability Test and Thermal Resistance*

The most common test for evaluating the flame-retardant qualities of coated sheets is the limiting oxygen index (LOI) test [48]. LOI is defined as the minimum oxygen concentration required for the combustion of materials in a mixture of nitrogen and oxygen. The blank paper's LOI value of 18.0 vol.% indicates that it is highly combustible. LOI values increased gradually with soaking time, and consequently with WPG, reaching 22.3 vol.% at 15 min (Table 3). While the LOI increase (18.0 to 22.3) is modest, it shifts the material from "highly flammable" toward the "combustible" threshold. The LOI values above atmospheric oxygen levels (~21%) indicate improved flame resistance. Although the enhancement is moderate, it remains significant for a thin, eco-friendly coating. This improvement can be attributed to the development of a protective silica layer that functions as a thermal barrier, restricting oxygen penetration and delaying heat transfer during combustion [49].

**Table 3:** Limiting oxygen index (LOI, vol.%) of uncoated and nano-silica/HEC-coated paper sheets (2% w/v impregnation solution) as a function of soaking time.

| Soaking Time, min. | Wt. Gained, % | LOI, vol.% |
|---|---|---|
| 0 | 0.000 | 18.00 |
| 2 | 22.65 | 21.50 |
| 5 | 26.16 | 21.90 |
| 10 | 27.45 | 22.00 |
| 15 | 35.27 | 22.30 |
| 20 | 26.29 | 21.80 |

Nano-silica promoted the formation of a stable protective char layer on the paper surface during combustion, reducing heat transfer and oxygen diffusion to the underlying cellulose [50]. The increase in LOI from 18.0 to 22.3 vol.% demonstrates improved flame resistance and reduced flammability of the coated paper

brcause LOI value is higher than the ambient air's oxygen concentration, which is roughly 21% [51]. However, these values remain within the combustible (slow-burning) range rather than indicating fully flame-retardant behavior. Therefore, the nano-silica/HEC coating provides a meaningful enhancement in fire performance while preserving the mechanical properties of the paper, making it a promising eco-friendly coating for improving paper safety.

Table 4 summarizes the performance of our nano-silica coating vs. other recent bio-based coating systems. Comprehensive evidence that nano-silica produced from rice husk waste improves the mechanical durability and chemical stability of paper sheets is shown by the combination of experimental characterization and DFT analysis, as well as by comparison with other studies (Table 4). Consequently, rice-husk-derived nano-silica provides an environmentally benign, sustainable method for improving the durability, performance, and safety of paper materials while simultaneously addressing agricultural waste management challenges.

**Table 4:** Comparative performance of bio-based and silica coatings for paper/cellulosic substrates.

| Coating Material | Silica Source/Base | Tensile Improvement | LOI/Barrier | Substrate | Reference |
|---|---|---|---|---|---|
| HEC/Nano-$SiO_2$ | Rice husk waste | +15%–25% | 18.0→22.3 vol.% | Rice straw/bagasse paper | Present study |
| Shellac/bentonite/alginate | Mineral/biopolymer | +10%–18% | Improved barrier | Bagasse paper | [1] |
| Bio-$SiO_2$ from RH + polymer matrix | Rice husk | Reported | Improved | Cellulosic sheets | [18] |
| Chitosan coating | Biopolymer | +8%–12% | Not reported | Kraft paper | [45] |
| Fire-retardant paper ($ZrO_2$/$SiO_2$) | Synthetic | Maintained | LOI > 30 vol.% | Specialty paper | [48] |
| GEL/AMP + silica gel (layer-by-layer) | Synthetic $SiO_2$ | +20% | LOI > 27 vol.% | Cotton fabric | [49] |

## 4 Conclusions

Amorphous nano-silica was successfully synthesized from rice husk waste through a multi-step process comprising controlled calcination at 450°C (3 h) and 800°C (2 h), alkaline extraction with 2.5 N NaOH, acid precipitation with 1 N HCl, and freeze-drying, yielding 93% $SiO_2$ from ash. This procedure is confirmed as an efficient, low-cost, and scalable route for converting rice husk waste into high-purity amorphous nano-silica, fully consistent with green chemistry and circular economy principles. FTIR and XRD analyses confirmed the formation of highly hydroxylated amorphous $SiO_2$ particles capable of forming strong hydrogen bonds with cellulose. SEM micrographs demonstrated uniform nanoparticle deposition on the paper surface, resulting in a continuous, compact coating layer that improves inter-fiber adhesion and surface integrity.

Maximum performance was obtained at soaking times of 10–15 min, where a WPG of 35.27% was achieved. Post-aging tensile strength and elongation improved by up to 25% and 94%, respectively, compared to uncoated paper. The LOI increased from 18.0 to 22.3 vol.%, and DFT calculations revealed that the energy gap widened from 1.342 to 1.803 eV while absolute hardness increased from 0.671 to 0.902 eV, confirming enhanced chemical stability and decreased susceptibility to oxidative degradation. These quantitative outcomes collectively demonstrate that nano-silica coating significantly improves the mechanical strength, thermal resistance, and anti-aging properties of paper materials, while maintaining a simple scalable process.

The primary mechanism underlying these improvements is the synergistic action of nano-silica Si–OH groups, which form hydrogen bonds with cellulose hydroxyl groups, and the HEC binder, which bridges adjacent fibers to promote cohesive inter-fiber bonding and uniform coating. Critically, the DFT analysis provides the first theoretical explanation of the anti-aging effect at the molecular orbital level for a rice-husk-derived nano-silica/cellulose system, linking the widening of the HOMO–LUMO gap directly to reduced susceptibility to oxidative and thermal degradation. The approach offers a sustainable pathway for valorizing rice husk waste into high-value nanomaterials, contributing to both green material innovation and circular economy objectives in the pulp and paper industry.

The limitations of this study include a primary focus on laboratory-scale synthesis and short-term accelerated aging. Further research should investigate long-term natural aging, coating uniformity, pilot-scale coating trials, surface chemistry mapping by XPS, precise silica quantification by TGA and elemental analysis, and the exploration of barrier properties, including water vapor transmission rate and oil resistance, for potential packaging applications.

**Acknowledgement:** The authors gratefully acknowledge the support of the National Research Centre (NRC), Egypt.

**Funding Statement:** The authors received no specific funding for this study.

**Author Contributions:** Mona A. El-Sabour: Conceptualization, Methodology, Investigation, Formal analysis, Writing—original draft. Mohamed El-Sakhawy: Supervision, Writing—review & editing, Validation, Investigation. Hebat-Allah S. Tohamy: Data curation, Methodology, Conceptualization, Data analysis, Resources, Investigation, Formal analysis. All authors reviewed and approved the final version of the manuscript.

**Availability of Data and Materials:** The authors confirm that the data supporting the findings of this study are available within the article.

**Ethics Approval:** Not applicable.

**Conflicts of Interest:** The authors declare no conflicts of interest.

## Nomenclature

| | |
|---|---|
| HEC | Hydroxyethyl cellulose |
| RH | Rice husk |
| SLS | Sodium lauryl sulfate |
| WPG | Weight percent gain |
| DFT | Density functional theory |

## References

1. Mohamed SAA, El-Sakhawy M, Diab MA. Enhancement of bagasse paper properties for sustainable packaging via bentonite and alginate loading in shellac coatings. Sci Rep. 2025;15(1):39412. doi:10.1038/s41598-025-22179-9.
2. Tétreault J, Bégin P, Paris-Lacombe S, Dupont AL. Modelling considerations for the degradation of cellulosic paper. Cellulose. 2019;26(3):2013–33. doi:10.1007/s10570-018-2156-x.
3. Zhu Z, Zhang K, Xue Y, Liu Z, Wang Y, Zhang Y, et al. Research on the structure and properties of traditional handmade bamboo paper during the aging process. Molecules. 2024;29(23):5741. doi:10.3390/molecules29235741.
4. He B, Zhao H, Li W, Meng L, Liu C, Fan H, et al. Enhancing capillary action of acidified paper to achieve uniform deacidification and long-lasting aging resistance. J Cult Herit. 2024;67(4):23–31. doi:10.1016/j.culher.2024.02.006.
5. Adak B, Baidya S, Teramoto Y. Biopolymers and their nanocomposites coated paper-based high barrier and sustainable food packaging materials. Carbohydr Polym. 2025;367(19):123966. doi:10.1016/j.carbpol.2025.123966.

6. Baskaran R, Thirugnanasambandham T. Advances in sustainable polymeric materials derived from renewable biopolymers integrated with nanotechnology for active food preservation: a review. Polym Plast Technol Mater. 2026;65(1):100–39. doi:10.1080/25740881.2025.2592713.
7. Sapuła P, Bialik-Wąs K, Malarz K. Are natural compounds a promising alternative to synthetic cross-linking agents in the preparation of hydrogels? Pharmaceutics. 2023;15(1):253. doi:10.3390/pharmaceutics15010253.
8. Ariga K, Lvov Y, Decher G. There is still plenty of room for layer-by-layer assembly for constructing nanoarchitectonics-based materials and devices. Phys Chem Chem Phys. 2022;24(7):4097–115. doi:10.1039/d1cp04669a.
9. Gunawardene OHP, Gunathilake C, Amaraweera SM, Fernando NML, Wanninayaka DB, Manamperi A, et al. Compatibilization of starch/synthetic biodegradable polymer blends for packaging applications: a review. J Compos Sci. 2021;5(11):300. doi:10.3390/jcs5110300.
10. Mohammadi X, Hossain A, Kontogiorgos V, Pratap-Singh A. Cold oxygen plasma-induced modifications in chitosan films: effects of solution and film treatment on structure and functionality. Food Hydrocoll. 2025;169(7):111572. doi:10.1016/j.foodhyd.2025.111572.
11. Wang S, Liu H, Liu G, Song P, Liu J, Liang Z, et al. Green superhydrophobic surfaces: from natural substrates to sustainable fabrication processes. Materials. 2025;18(18):4270. doi:10.3390/ma18184270.
12. Vasile C. Polymeric nanocomposites and nanocoatings for food packaging: a review. Materials. 2018;11(10):1834. doi:10.3390/ma11101834.
13. Babaei-Ghazvini A, Acharya B. The effects of aspect ratio of cellulose nanocrystals on the properties of all CNC films: tunicate and wood CNCs. Carbohydr Polym Technol Appl. 2023;5(6):100311. doi:10.1016/j.carpta.2023.100311.
14. Dlomo K, Mohomane SM, Motaung TE. Influence of silica nanoparticles on the properties of cellulose composite membranes: a current review. Cellul Chem Technol. 2020;54(7–8):765–75. doi:10.35812/cellulosechemtechnol.2020.54.76.
15. Hamidu I, Afotey B, Kwakye-Awuah B, Anang DA. Synthesis of silica and silicon from rice husk feedstock: a review. Heliyon. 2025;11(4):e42491. doi:10.1016/j.heliyon.2025.e42491.
16. Taiye MA, Hafida W, Kong F, Zhou C. A review of the use of rice husk silica as a sustainable alternative to traditional silica sources in various applications. Env Prog and Sustain Energy. 2024;43(6):e14451. doi:10.1002/ep.14451.
17. Chun J, Gu Y, Hwang J, Oh KK, Lee JH. Synthesis of ordered mesoporous silica with various pore structures using high-purity silica extracted from rice husk. J Ind Eng Chem. 2020;81:135–43. doi:10.1016/j.jiec.2019.08.064.
18. Shen Y. Rice husk silica derived nanomaterials for sustainable applications. Renew Sustain Energy Rev. 2017;80:453–66. doi:10.1016/j.rser.2017.05.115.
19. Pearson RG. Chemical hardness and density functional theory. J Chem Sci. 2005;117(5):369–77. doi:10.1007/BF02708340.
20. El-Sakhawy M, Adel AM, Diab MA, Al-Shemy M. Facile methods for the preparation of micro- and mesoporous amorphous silica from rice husk. Biomass Convers Biorefin. 2022;12(10):4709–18. doi:10.1007/s13399-020-01112-2.
21. Islam MT, Hossen MF, Kudrat-E-Zahan M, Ali Asraf M, Zakaria CM, Hayatullah, et al. Effect of temperature and time on purity, morphology and phase transformations of silica from rice husk. Chem Inorg Mater. 2025;5(3):100092. doi:10.1016/j.cinorg.2025.100092.
22. ASTM D2863-19. Standard test method for measuring the minimum oxygen concentration to support candle-like combustion of plastics (oxygen index). West Conshohocken, PA, USA: ASTM International; 2019.
23. Pearson RG. Absolute electronegativity and hardness: application to inorganic chemistry. Inorg Chem. 1988;27(4):734–40. doi:10.1021/ic00277a030.
24. Ellerbrock R, Stein M, Schaller J. Comparing amorphous silica, short-range-ordered silicates and silicic acid species by FTIR. Sci Rep. 2022;12(1):11708. doi:10.1038/s41598-022-15882-4.
25. Fernandes IJ, Calheiro D, Sánchez FAL, Camacho ALD, de Campos Rocha TLA, Moraes CAM, et al. Characterization of silica produced from rice husk ash: comparison of purification and processing methods. Mater Res. 2017;20(suppl 2):512–8. doi:10.1590/1980-5373-mr-2016-1043.
26. McLean B, Yarovsky I. Structure, properties, and applications of silica nanoparticles: recent theoretical modeling advances, challenges, and future directions. Small. 2024;20(51):e2405299. doi:10.1002/smll.202405299.

27. Zhuravlev LT. The surface chemistry of amorphous silica. Zhuravlev model. Colloids Surf A Physicochem Eng Asp. 2000;173(1–3):1–38. doi:10.1016/S0927-7757(00)00556-2.
28. Ong HR, Iskandar WM, Chong J, Khan MM, Ong TK, Chua BK. Investigation on silane concentration of $SiO_2$ nanoparticle: FTIR analysis. Chem Eng Trans. 2023;106:1345–50.
29. Nascimento ACK. Study of rice husk ash by infrared spectroscopy. Int J Sci Eng Investig. 2020;9(101):60–2. doi:10.1016/0040-6031(80)87160-7.
30. Ke X, Wu Z, Lin J, Wang F, Li P, Xu R, et al. A rapid analytical method for the specific surface area of amorphous $SiO_2$ based on X-ray diffraction. J Non Cryst Solids. 2020;531:119841. doi:10.1016/j.jnoncrysol.2019.119841.
31. Khouchaf L, Boulahya K, Das PP, Nicolopoulos S, Kis VK, Lábár JL. Study of the microstructure of amorphous silica nanostructures using high-resolution electron microscopy, electron energy loss spectroscopy, X-ray powder diffraction, and electron pair distribution function. Materials. 2020;13(19):4393. doi:10.3390/ma13194393.
32. Shinohara Y, Kohyama N. Quantitative analysis of tridymite and cristobalite crystallized in rice husk ash by heating. Ind Health. 2004;42(2):277–85. doi:10.2486/indhealth.42.277.
33. Della VP, Kühn I, Hotza D. Rice husk ash as an alternate source for active silica production. Mater Lett. 2002;57(4):818–21. doi:10.1016/S0167-577X(02)00879-0.
34. Kalapathy U, Proctor A, Shultz J. An improved method for production of silica from rice hull ash. Bioresour Technol. 2002;85(3):285–9. doi:10.1016/s0960-8524(02)00116-5.
35. Ruiz-Cañas MC, Corredor LM, Quintero HI, Manrique E, Romero Bohórquez AR. Morphological and structural properties of amino-functionalized fumed nanosilica and its comparison with nanoparticles obtained by modified stöber method. Molecules. 2020;25(12):2868. doi:10.3390/molecules25122868.
36. Mohamed A, Visco DP Jr, Breimaier K, Bastidas DM. Effect of molecular structure on the B3LYP-computed HOMO-LUMO gap: a structure-property relationship using atomic signatures. ACS Omega. 2025;10(3):2799–808. doi:10.1021/acsomega.4c08626.
37. Parr RG, Chattaraj PK. Principle of maximum hardness. J Am Chem Soc. 1991;113(5):1854–5. doi:10.1021/ja00005a072.
38. Castelli IE, Man IC, Soriga SG, Parvulescu V, Halck NB, Rossmeisl J. Role of the band gap for the interaction energy of coadsorbed fragments. J Phys Chem C. 2017;121(34):18608–14. doi:10.1021/acs.jpcc.7b04974.
39. Khan A, Abas Z, Kim H, Kim J. Recent progress on cellulose-based electro-active paper, its hybrid nanocomposites and applications. Sensors. 2016;16(8):1172. doi:10.3390/s16081172.
40. Chen H, Wang B, Li J, Ying G, Chen K. High-strength and super-hydrophobic multilayered paper based on nano-silica coating and micro-fibrillated cellulose. Carbohydr Polym. 2022;288(31):119371. doi:10.1016/j.carbpol.2022.119371.
41. Deshwal GK, Panjagari NR, Alam T. An overview of paper and paper based food packaging materials: health safety and environmental concerns. J Food Sci Technol. 2019;56(10):4391–403. doi:10.1007/s13197-019-03950-z.
42. Sampson WW. Materials properties of paper as influenced by its fibrous architecture. Int Mater Rev. 2009;54(3):134–56. doi:10.1179/174328009x411154.
43. Larsson PT, Lindström T, Carlsson LA, Fellers C. Fiber length and bonding effects on tensile strength and toughness of kraft paper. J Mater Sci. 2018;53(4):3006–15. doi:10.1007/s10853-017-1683-4.
44. Niknejad E, Jafari R, Valipour Motlagh N. Mechanical properties of biodegradable fibers and fibrous mats: a comprehensive review. Molecules. 2025;30(15):3276. doi:10.3390/molecules30153276.
45. Vikele L, Laka M, Sable I, Rozenberga L, Grinfelds U, Zoldners J, et al. Effect of chitosan on properties of paper for packaging. Cellul Chem Technol. 2017;51(1–2):67–73.
46. Hubbe MA, Gill RA. Fillers for papermaking: a review of their properties, usage practices, and their mechanistic role. BioResources. 2015;11(1):2886–963. doi:10.15376/biores.11.1.2886-2963.
47. Małachowska E, Pawcenis D, Dańczak J, Paczkowska J, Przybysz K. Paper ageing: the effect of paper chemical composition on hydrolysis and oxidation. Polymers. 2021;13(7):1029. doi:10.3390/polym13071029.
48. Dong LY, Zhu YJ. Fire-retardant paper with ultrahigh smoothness and glossiness. ACS Sustain Chem Eng. 2020;8(47):17500–7. doi:10.1021/acssuschemeng.0c06665.

49. Zhang X, Li D, You F, Li G, Zhou C, Cheng D, et al. Improved thermal stability and flame retardancy levels of cotton fabrics treated by GEL/AMP layer-by-layer assembly and silica gel composite coatings. Cellulose. 2023;30(10):6695–718. doi:10.1007/s10570-023-05278-6.
50. He SM, Wang F, Zhang L, Zhang JY, Zeng FR, Liu BW, et al. Quick and efficient flame-retardant, antibacterial and antifungal treatment for high-performance cellulose paper. Prog Org Coat. 2023;185:107947. doi:10.1016/j.porgcoat.2023.107947.
51. Kiliaris P, Papaspyrides CD. Polymer/layered silicate (clay) nanocomposites: an overview of flame retardancy. Prog Polym Sci. 2010;35(7):902–58. doi:10.1016/j.progpolymsci.2010.03.001.